



**HAL**  
open science

## Kinetic modeling of deep vacuum residue hydroconversion in a pilot scale continuous slurry reactor with recycle

Barbara Browning, Françoise Couenne, Tim Jansen, Maxime Lacroix, Pedro Alvarez, Mélaz Tayakout-Fayolle

► **To cite this version:**

Barbara Browning, Françoise Couenne, Tim Jansen, Maxime Lacroix, Pedro Alvarez, et al.. Kinetic modeling of deep vacuum residue hydroconversion in a pilot scale continuous slurry reactor with recycle. *Chemical Engineering Journal Advances*, 2020, 4, pp.100063. 10.1016/j.cej.2020.100063 . hal-03084497

**HAL Id: hal-03084497**

**<https://hal.science/hal-03084497>**

Submitted on 15 Dec 2022

**HAL** is a multi-disciplinary open access archive for the deposit and dissemination of scientific research documents, whether they are published or not. The documents may come from teaching and research institutions in France or abroad, or from public or private research centers.

L'archive ouverte pluridisciplinaire **HAL**, est destinée au dépôt et à la diffusion de documents scientifiques de niveau recherche, publiés ou non, émanant des établissements d'enseignement et de recherche français ou étrangers, des laboratoires publics ou privés.



Distributed under a Creative Commons Attribution - NonCommercial 4.0 International License

## **Kinetic Modeling of Deep Vacuum Residue Hydroconversion in a Pilot Scale Continuous Slurry Reactor with Recycle**

Barbara Browning<sup>a\*</sup>, Françoise Couenne<sup>a</sup>, Tim Jansen<sup>b</sup>, Maxime Lacroix<sup>b</sup>, Pedro Alvarez<sup>b</sup>,  
Mélaz Tayakout-Fayolle<sup>a</sup>

<sup>a</sup> Univ Lyon, Université Claude Bernard Lyon 1, CNRS, LAGEPP UMR 5007, 43 boulevard du 11 novembre 1918, F-69100, VILLEURBANNE, France

<sup>b</sup> TOTAL Research and Technology Gonfreville, Zone Industrielle du Havre, BP27, 76700 Harfleur, France

\* Corresponding author

barbara.browning@univ-lyon1.fr      tel: +33 4 72 43 18 70

### **Abstract**

Slurry phase hydroconversion is a developing technology with the potential to completely upgrade Vacuum Residues (VR). In this work we use data from a continuous pilot plant with recycle to test and extend an existing distributed lumped kinetic model. The new data includes results from 134 steady state experiments with a Heavy Iran VR, including some at very high conversion, and allows sediment production rates to be quantified as well as sulphur removal in the form of H<sub>2</sub>S. The purpose of the work is to study the impact of the deep conversion reaction conditions and feedstock on the reaction kinetics. The model uses nineteen distributed lumps to represent the heavy hydrocarbons undergoing hydroconversion and hydrodesulphurisation with VR defined as the boiling range > 525°C. Reaction rates are based on molar concentrations. Hydrogen consumption and sediment production are taken into account in the model, as well as vapour liquid mass transfer resistances and vapour-liquid equilibrium. Parameter estimation has been carried out and the model provides a good fit with the experimental data. The modelling exercise found that, at very high conversions, thermal reactions give way to a cascade of catalytic reactions. The model gave a moderate fit for hydrogen consumption rates, which are strongly dependent on

feedstock. Accumulation of sediment at high conversions was identified and well represented and the description of hydrodesulfurisation rates as proportional to cracking rates was validated.

Keywords: kinetic modeling; slurry phase hydroconversion; distributed lumped model; vacuum residue; continuous reactor; recycle

## 1. Introduction

As part of the energy transition, oil product demand is shifting towards the lighter cuts required for petrochemical feedstocks, aviation and shipping [1]. This challenge is amplified by the fact that crude sources are becoming heavier [2]. Slurry phase hydroconversion processes have the potential to help bridge the gap by upgrading very heavy residues, with high asphaltenes and impurities content, to near total conversion [3].

Vacuum Residue (VR) is the heaviest crude oil distillation product and includes everything with an atmospheric boiling point above 525 °C. This material has high viscosity and low hydrogen to carbon ratio. There are two main VR upgrading routes: carbon rejection and hydrogen addition [4]. Carbon rejection processes are the simplest and least expensive option, as no catalyst or H<sub>2</sub> supply is needed, but higher conversions are achieved with hydrogen addition methods. These processes have the benefit of avoiding coke production but are traditionally dependent on supported catalysts. With very heavy residues, this leads to high reactor pressure drop, fouling and feed diffusion and mass transfer problems [4]. Slurry phase hydroconversion adopts unsupported dispersed catalysts, sometimes formed in-situ, to overcome these difficulties [5]. It is an active area of research with numerous recent studies on catalyst improvements and innovations [6–9].

Several reviews [4,5,10,11] follow the recent evolution in slurry phase VR hydroconversion technologies, the most well-known of which are listed in Table 1. Operating conditions are

above 400°C and 100 bar with reported conversions of at least 90%. The historical Veba-Combi-Cracking (VCC) process, along with the Eni Slurry Technology (EST) process, is a licensed technology [12,13]. Slurry processes can be classified into two groups by catalyst type: low cost / high concentration (Ex: Fe based) or high cost / low concentration (Ex: Mo based). Of those in Table 1 only VCC falls into the first category.

A refinery scale slurry phase reactor is similar to a bubble column and contains dispersed catalyst suspended in the liquid phase with co- or counter-current gas flow [16]. The molecular complexity of VR means that its components comprise a wide range of activities and, to achieve deep conversion, the processes tend to include a strategy to increase concentration and residence time of the most refractory compounds. Coming back to the processes listed in Table 1, the VCC process valorises unreacted residue through combustion or coking [14] and the Chevron LC-Slurry process concentrates refractory components through sequential multi-stage reactors and an inter-stage separator. Recycle of unconverted residue is an option with the added benefit of conserving active catalyst within the reactor system [12,15], but a potential drawback is the accumulation of large agglomerated catalyst crystallites [15]. The UOP Uniflex process is reported both with and without a Heavy Vacuum Gas Oil (HVGO) recycle [10,15]. The PVDSA Intevap HDH plus process has an optional recycle stream, reported to increase conversion from 91 to 97%. Headwaters Technology Innovation HCAT/(HC)<sub>3</sub> and the EST processes both recycle unconverted residue back to the reactor [10,12].

**Table 1. VR Slurry phase hydroconversion upgrading processes**

Process name	Reactor conditions		Conversion	Type of process
	Temperature (°C)	Pressure (bar)		
Veba-Combi-Cracker (VCC) [12,14]	440-485	220-250	>90	Once-through with 5 wt% iron based catalyst [13].
UOP Uniflex (CANMET) [13,15]	450-460	160-180	97	Once-through or recycle
Eni Slurry Technology (EST) [12]	410-450	150	95-99	Recycle
PVDSA-Intevap HDH plus [12,15]	430-460	170-210	92	Optional recycle increases conversion to 97%
Chevron LC-Slurry [13,15]	400-440	100-200	97	Sequential multi-stage reactors with inter-stage separator and possible recycle
Headwaters Technology Innovation HCAT/(HC)3 [10,13,15]	430-450	140	95	Recycle

Laboratory and pilot scale studies of continuous VR slurry phase deep hydroconversion are rare [3]. Continuous reactors have been used with VR to test slurry phase hydroconversion catalysts [17–19], alternative catalyst systems [20,21] and catalytic steam cracking [22–24]. Jansen et al. performed slurry phase hydroconversion experiments with an atmospheric residue in a continuous micro-pilot with recycle and simulated the results [25,26] and Alvarez et al. extended this to VR for a range of operating temperatures, residence times and recycle ratios [27]. The impact of the recycle stream has been simulated with batch and semi-batch reactors by returning some [28] or all [29,30] of the reaction products to the reactor and reprocessing them several times. Also, hydroconversion products have been combined with fresh feed and then reprocessed [31–33]. Bellussi et al. [34] describe a pilot scale 7.5 L ebullated bed slurry reactor with a continuous recycle and fractionation system. In general, as residue is recycled, it becomes more refractory to processing. The molecular weight, hydrogen content and reactivity of the residue are reduced and the aromaticity increases. Asphaltenes content degrades in two stages. Firstly, branches detach, resulting in very stable polyaromatic hydrocarbons with high boiling points. Then, under sufficiently severe operating conditions these, more resistant, components break down [32] and complete conversion of the residue is possible [28].

Quitian and Ancheyta discuss kinetic models for slurry phase hydrocracking of residue feedstocks [35] and Al-Attas et al. list some models proposed in the literature [11]. There are few kinetic models for slurry phase hydroconversion [27,36,37] but many for hydrocracking, with good reviews by Ancheyta [38] and Thybaut and Marin [39]. Strategies to represent reaction components range from simple traditional lumping, through microkinetics to complex molecular reconstruction with the level of detail dependent on the available data and time for computation. Single-Event MicroKinetics (SEMK) models for hydrocracking build

large kinetic networks up from the elementary reaction steps and control the number of parameters by relumping rate coefficients for similar steps or species [39]. Molecular-level kinetic models, such as those developed by Klein's research group, liken residue to a cross-linked polymer with cores, inter-core linkages and side chains. Reaction rates are determined from probability density functions of these structural attributes [40–42]. Rueda-Velasquez and Gray [43] and Oliveira et al. [44] developed similar methods and molecular-level kinetic models have also been applied to other refinery processes with good results [45,46]. These models have intensive analysis requirements. For example, Chen et al. [46] used data from six types of analysis method: density, number average molecular weight, Conradson carbon residue, elemental, mass spectrometry and simulated distillation.

At the other end of the spectrum are traditional lumped models, with five or six pseudo-components. These are useful for catalyst screening and process optimization [39] or testing new reactor models [47]. Reaction rate parameters are estimated for each lump and, generally, valid for one feedstock and set of operating conditions [39]. It is difficult to extend traditional lumped models because every additional lump requires an accompanying set of parameters. Another limitation is that the heaviest lump has no upper boiling point limit and includes a very wide range of different components, so that it cannot be assumed to have constant physical properties. To overcome this, the lump can be represented as a series of pseudo-components [36,48]. Distributed and continuous lumped models, such as those of Stangeland [49] and Laxaminarasimhan et al. [50], were developed to add detail whilst containing the number of parameters. In particular, Stangeland's model [49], which combines 22 distributed lumps, four parameters, a cracking rate function and product distribution, has been extended to include the effect of H<sub>2</sub> partial pressure on reaction rates [51] and has proven useful to represent hydrocracking kinetics in industrial scale reactors [52–54].

Browning et al. [36] previously developed a distributed lump kinetic model for slurry phase VR hydroconversion with vapour liquid mass transfer resistances and equilibrium taken into account. This was validated against results from experiments performed in a laboratory scale semi-batch reactor and was a stepping stone towards a model which could include the very high conversions achieved with a recycle stream. The experimental results used in this work come from a continuous hydroconversion slurry pilot operating in recycle mode. Conditions are more severe than could be generated in the previously used laboratory scale semi-batch reactor and are close to those found in a refinery scale slurry phase hydroconversion reactor. Furthermore, the scale of the pilot plant allowed analysis of the small quantity of sediment found in the product stream. The objective of this work is to improve the model of Browning et al. [36] by extending it to include Hydrodesulfurisation (HDS) as an integral part of the model, as opposed to its previous representation as a side reaction, and also extending the model to the pilot operating conditions and quantifying the sediment production rate. Parameter estimation is carried out and the results are discussed and compared to the experimental data from the hydroconversion slurry pilot. The benefits of a kinetic model validated for refinery conditions will be greater ability to predict plant outputs and to simulate and optimise real operating conditions.

## **2. Material and methods**

### **2.1. Experimental set-up**

Slurry phase hydroconversion experiments were performed in a pilot with 2 x 2.2L continuous reactors and a downstream separation and recycle section. Figure 1 gives a simplified flow diagram of the equipment. Operation is possible with one or two reactors online and in once-through or recycle mode. Campaigns of experiments were carried out where the first set of operating conditions were always in once-

through mode and recycle rates could be specified from the second experiment to the end of the campaign. The separation section includes a high pressure separator and a stripper operating at atmospheric pressure. Gases and condensate streams pass through a scrubber and low pressure separator before analysis. Liquids are collected in a reservoir before recycle back to the reactors. The feedstock was an Iran Heavy VR with 4.2 wt % sulphur content and density of  $1053 \text{ kg.m}^{-3}$  at  $15^\circ\text{C}$  and atmospheric pressure. This was mixed with a catalyst precursor and  $\text{H}_2$  at 150 bar upstream of the reactor. Operating temperatures ranged from  $420$  to  $452^\circ\text{C}$  with feed flow rates from  $0.27 \text{ kg.h}^{-1}$  to  $1.23 \text{ kg.h}^{-1}$  in once through mode. Recycle rates are up to 3.2 times the feed mass flow rate. Outlet gases were analysed online by gas chromatography. All condensate and residue liquid products were analysed by High Temperature Simulated Distillation (HTSD) using an Agilent series 6890 chromatography column and according to the standard ASTM guideline D7169 [55]. Sediment quantities were measured by precipitation in tetrahydrofurane and the amount of  $\text{H}_2$  consumed was determined by analysis of the reaction products. In once-through mode, density measurement was by pycnometer and steady state was confirmed by processing until the same result was obtained for two successive samples. For recycle operation, the residue density and outlet flow rate were measured by a Coriolis meter which allowed steady state operation to be verified. Mass balance data was accurate to  $\pm 5\%$ .

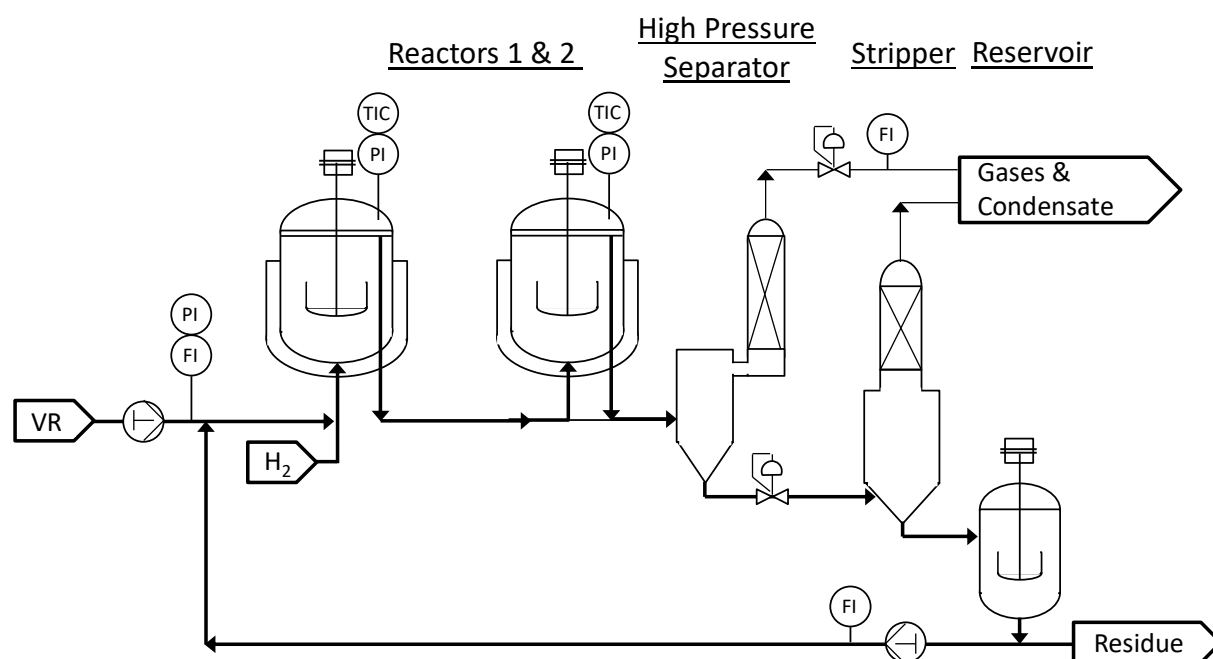


Figure 1. Simplified Process Flow Diagram of slurry phase hydroconversion pilot plant.

## 2.2. Experimental results

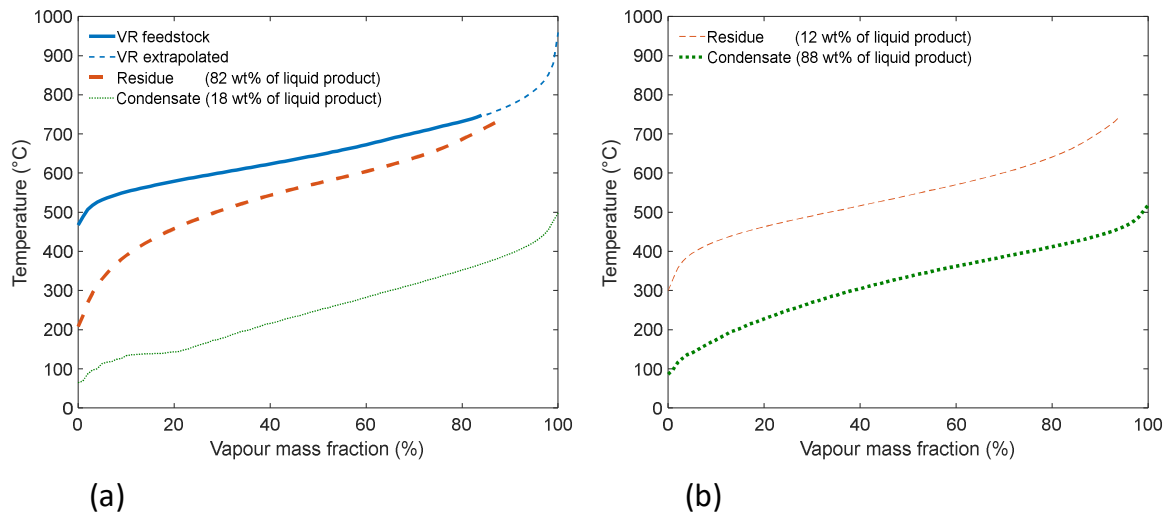
134 experiments were carried out in 12 campaigns in both once-through and recycle mode and with one and two reactors in operation as listed in Table 2.

Table 2. Campaigns performed with hydroconversion pilot plant.

Campaign number	Number of reactors in operation	Sediment measurement	Operating mode	
			Experiment 1	Subsequent experiments
1-3	1	N	Once-through	Once-through
4	1	N	Once-through	Recycle
5	2	N	Once-through	Recycle
6	2	N	Once-through	Recycle
7-12	2	Y	Once-through	Recycle

Figure 2 gives HTSD results for the feedstock and typical liquid products at 49% and 94% conversion. HTSD allows analysis of heavy oils up to an atmospheric equivalent boiling point of 749°C [56]. The composition above this was estimated by the extrapolation method described in Riazi [57]. This uses Eq. (1) to complete the HTSD data for the whole boiling range, with the boiling point and initial boiling points,  $T_b$  and  $T_{b0}$  in Kelvin, A and B constant and  $x_c$  the distilled fraction. The composition of the residue and condensate liquid products is similar for both conversions shown. However, at 49% conversion, 81% of the liquid product is residue whereas at 94% conversion this drops to 12% with 88% recovered as condensate.

$$\frac{T_b - T_{b0}}{T_{b0}} = \left[ \frac{A}{B} \ln \left( \frac{1}{1 - x_c} \right) \right]^{\frac{1}{B}} \quad (1)$$



**Figure 2. Typical HTSD results at (a) 49% (b) 94% conversion. Feedstock, residue and condensate represented by solid, dashed and dotted lines respectively.**

### 3. Model Construction

Figure 3 gives the flow diagram used to simulate the slurry phase hydroconversion pilot plant. Physical properties are calculated at the temperatures shown. The reactors were represented as two CSTRs (CSTR 1 and CSTR 2) with the following assumptions:

- Isothermal operation
- All reactions occur in the liquid phase,
- Mass transfer between liquid and vapour phases,
- Perfect mixing in the reactor liquid and vapour phases,
- The vapour phase is considered an ideal gas and the liquid as an ideal solution

The rest of the system was represented using simple standard units. The choice to use a splitter and plug flow reactors was for simplicity and because it was adapted to the data available. The real pilot plant separation system between the reactors and the reservoir comprised a stripper and several other pieces of equipment, operating at different temperatures and pressures (see Figure 1). No equilibrium data was available but the outlet residue, gas and condensate stream compositions were measured. Since the overall experimental separation was known, we used this data to estimate the split for each lump over a range of operating conditions.

Having estimated the overall split we added the two plug flow reactors to take account of the volumes in the system. PFR 1 represents the delay due to the separation system residence time and PFR2 that of the recycle pipeline.

The reservoir was modelled as a continuous stirred tank.

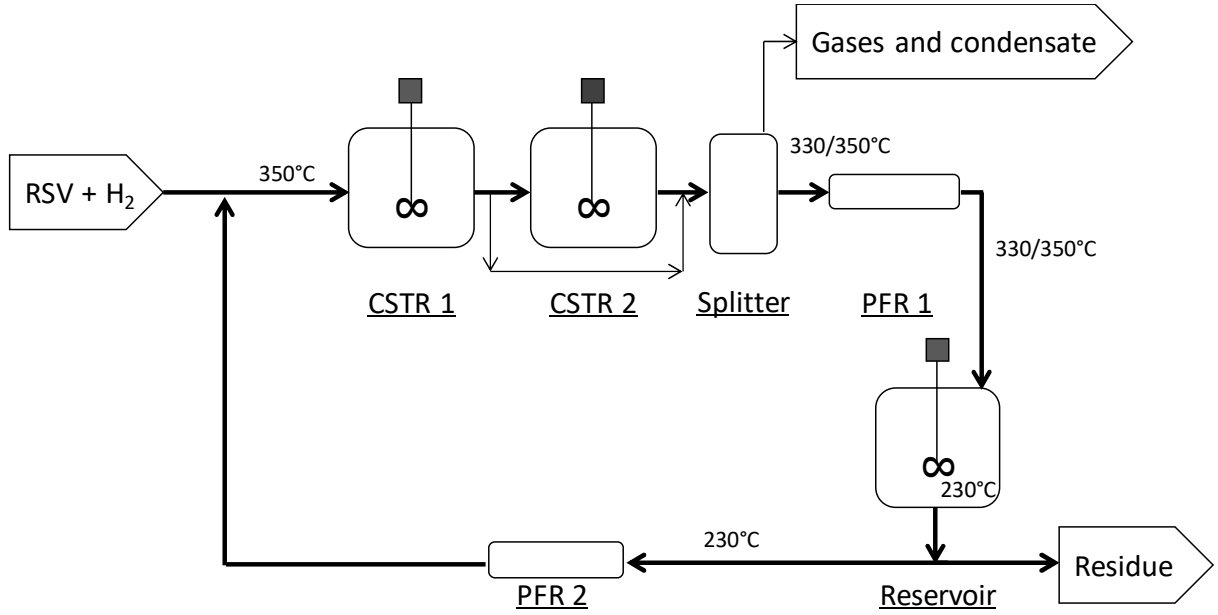


Figure 3. Flow diagram for slurry phase hydroconversion pilot plant simulation.

### 3.1 Reactor model

Overall and component mole balances were calculated for the liquid and vapour phases according to Eq.s (2) to (6), where the subscripts *in* and *out* relate to the reactor inlet and outlet streams. Concentrations,  $C$ , are in  $\text{mol.m}^{-3}$ , Volumes,  $V$ , in  $\text{m}^3$ , volumetric flowrates,  $Q$ , in  $\text{m}^3.\text{s}^{-1}$  and vapour liquid mass transfer rates,  $F_{ex}$ , are in  $\text{mol.s}^{-1}$ . Finally reaction rates,  $r$ , are in  $\text{mol.s}^{-1}.\text{m}^{-3}$  and  $V_{mol,i}$  is the molar volume of the lump,  $i$ , in  $\text{m}^3.\text{mol}^{-1}$ .  $L$  and  $g$  refer to liquid and gas phases and  $i$  and  $T$  indicate individual lumps and total quantity.

Component liquid phase:

$$C_i^L \frac{dV_L}{dt} + V_L \frac{dC_i^L}{dt} = C_{i,in}^L Q_{V,in}^L - C_i^L Q_{V,out}^L + V_L r_i + F_{ex,i} \quad (2)$$

Overall liquid phase:

$$C_T^L \frac{dV_L}{dt} + V_L \frac{dC_T^L}{dt} = C_{T,in}^L Q_{V,in}^L - C_T^L Q_{V,out}^L + V_L r_T + F_{ex,T} \quad (3)$$

Component gas phase:

$$C_i^g \frac{dV_g}{dt} + V_g \frac{dC_i^g}{dt} = C_{i,in}^g Q_{V,in}^g - C_i^g Q_{V,out}^g - F_{ex,i} \quad (4)$$

Overall liquid and gas phases:

$$\begin{aligned} C_T^L \frac{dV_L}{dt} + V_L \frac{dC_T^L}{dt} + C_T^g \frac{dV_g}{dt} + V_g \frac{dC_T^g}{dt} \\ = C_{T,in}^g Q_{V,in}^g - C_T^g Q_{V,out}^g + C_{T,in}^L Q_{V,in}^L - C_T^L Q_{V,out}^L + V_L r_T \end{aligned} \quad (5)$$

Reactor liquid volume is calculated using the molar volumes and based on the assumption that the liquid is an ideal solution:

$$\frac{dV_L}{dt} = V_L \frac{\sum V_{mol,i} \frac{dC_i^L}{dt}}{(1 - \sum V_{mol,i} C_i^L)} \quad (6)$$

The reactor liquid volumes are controlled by overflow into the outlet pipe and the gas volume fraction,  $\varepsilon_g$ , is related to the volumetric gas flow rate,  $Q_V^g$ , in  $\text{m}^3 \cdot \text{s}^{-1}$ , through the reactor by an in-house correlation in the form of Eq. (7) with a and b constant. Vapour liquid mass transfer rates,  $F_{ex,i}$ , in  $\text{mol} \cdot \text{s}^{-1}$ , are found from Eq. (8) with  $C_i^L$  and  $C_i^{L*}$ , in  $\text{mol} \cdot \text{m}^{-3}$ , the liquid concentrations in the reactor and at equilibrium.  $V_L$ , in  $\text{m}^3$ , is the liquid volume and  $k_l a$ , in  $\text{s}^{-1}$ , the vapour liquid mass transfer coefficient.

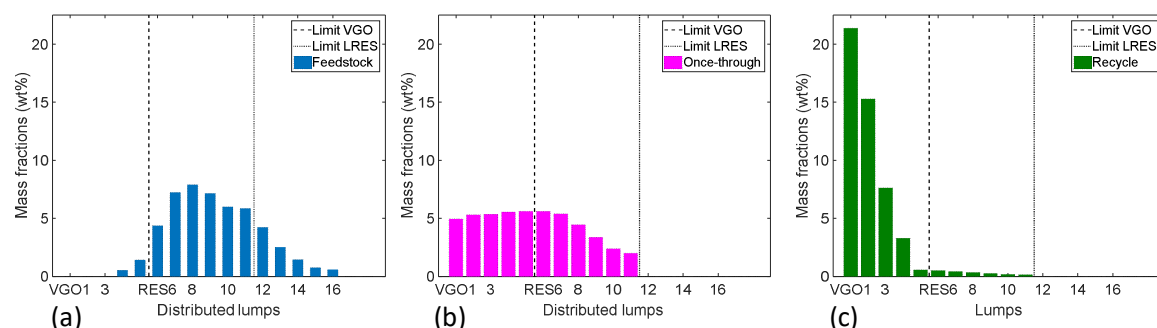
$$\varepsilon_g = a \cdot (Q_V^g)^b \quad (7)$$

$$F_{ex,i} = V_L k_l a (C_i^{L*} - C_i^L) \quad (8)$$

### 3.2 Kinetic model

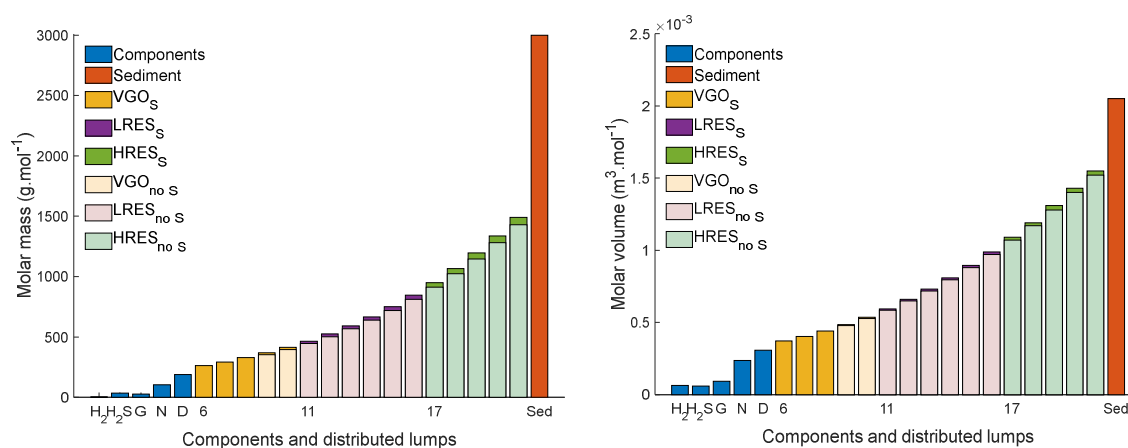
The kinetic model is based on our previous work [36]. True boiling points were used to define traditional lumps as GAS ( $T_b < 36^\circ\text{C}$ ), NAPH ( $36^\circ\text{C} < T_b < 160^\circ\text{C}$ ), DIST ( $160^\circ\text{C} < T_b < 350^\circ\text{C}$ ), VGO ( $350^\circ\text{C} < T_b < 525^\circ\text{C}$ ) and RES ( $525^\circ\text{C} +$ ). The VGO and RES lumps were then subdivided into distributed lumps of boiling range  $35^\circ\text{C}$ : VGO<sub>*i*</sub> with *i* = 1 to 5, LRES<sub>*i*</sub> with *i* = 6 to 11 and HRES<sub>*i*</sub> with *i* = 12 to 16. The Heavy Iran VR feedstock is composed of distributed lumps VGO<sub>4</sub> to HRES<sub>16</sub>. LRES<sub>*i*</sub> and HRES<sub>*i*</sub> are considered separately based on our observations of their disappearance rates. Note also that the cut point between LRES<sub>*i*</sub> and HRES<sub>*i*</sub> is  $735^\circ\text{C}$  which is very close to the maximum boiling point for HTSD. So, LRES<sub>*i*</sub> quantities are measured whereas HRES<sub>*i*</sub> are mostly estimated using the Riazi method [57]. Figure 4 gives the feedstock mass distribution after lumping as well as typical pilot plant liquid products in once-through and recycle mode without extrapolation of the HTSD analysis

results. To incorporate HDS into the distributed lumped model a second similar set of reduced sulphur distributed lumps with the same boiling ranges was also defined: VGO\_low\_Si, LRES\_low\_Si and HRES\_low\_Si.

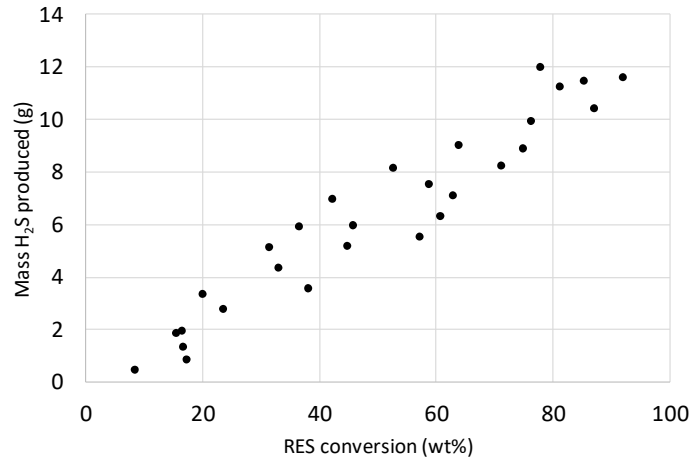


**Figure 4. Distributed lump mass fractions for (a) feedstock and typical liquid products in (b) once-through and (c) recycle modes.**

Molar masses and volumes are required for each component, including the distributed lumps, and these were estimated using ProSimPlus 3.3 [36]. To calculate the molar masses and volumes of the reduced sulphur lumps it was assumed that the sulphur mass distribution is uniform across the feedstock and that the atomic sulphur volume is additive with the volume of the sulphur free distributed lump. Figure 5 gives the results for all the lumps.



**Figure 5. Calculated molar masses and molar volumes of hydrocarbon lumps with and without sulphur content.**



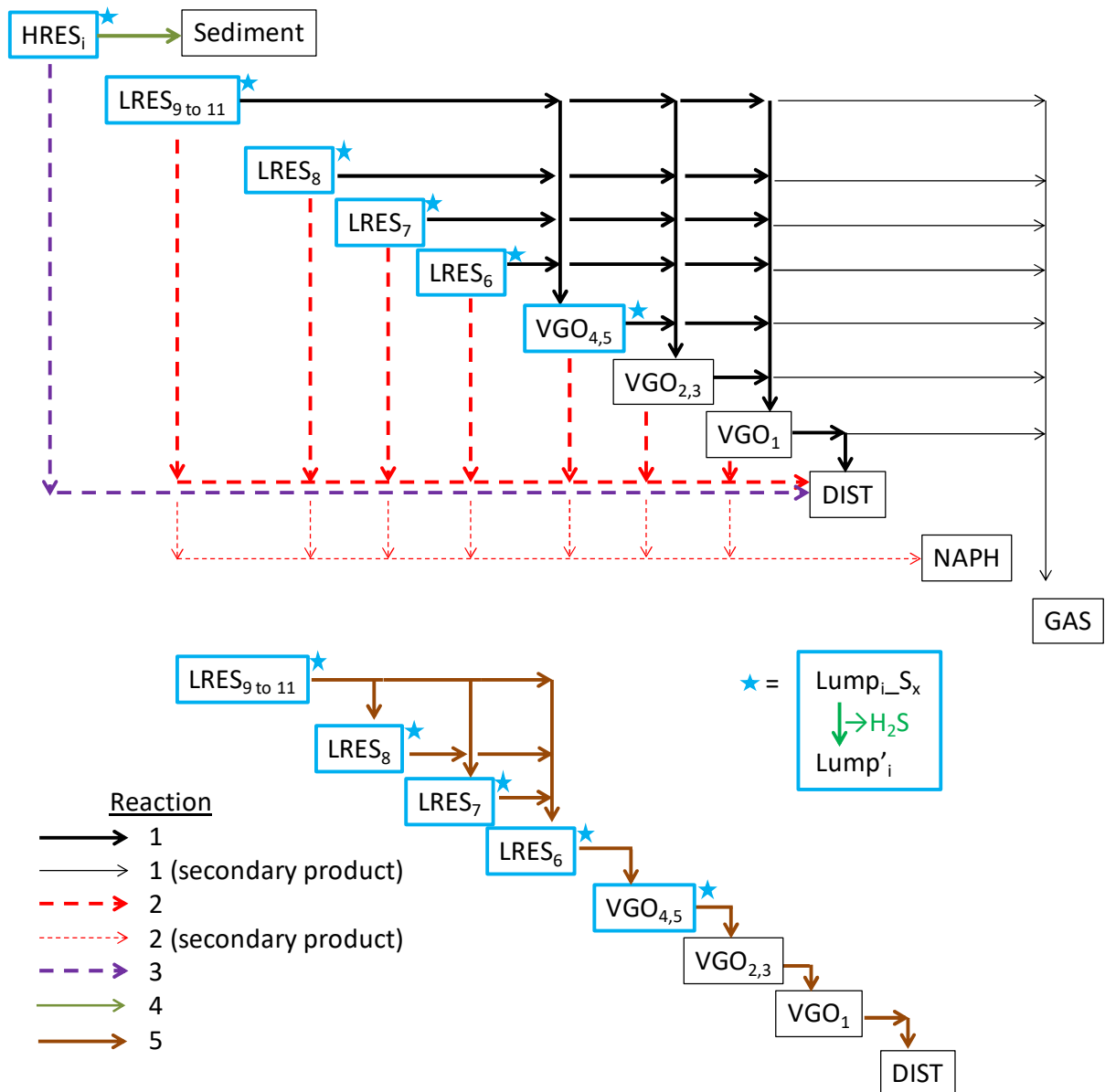
**Figure 6. H<sub>2</sub>S production against residue conversion results from semi-batch reactor [36].**

Figure 6 compares H<sub>2</sub>S production against residue conversion for slurry phase hydroconversion in a semi-batch reactor [36]. The relation appears almost linear and this is used later in the development of the kinetic model. The reaction scheme, shown in Figure 7, is based on our previous work [36]. It comprises five sets of hydrocracking reactions, where each step is considered individually, and incorporates HDS. The reactions are listed in Eq.s (10) to (19). The cracking reactions all consume H<sub>2</sub> and produce lighter gas oil products. Reactions 1 to 4 are thermally activated and reaction 5 is a catalytic cascade. HDS releases sulphur in the form of H<sub>2</sub>S and transfers material from the sulphur-containing, distributed lumps used to represent the feedstock to the reduced-sulphur lumps. Both the sulphur containing and sulphur reduced lumps undergo the same hydrocracking reactions. The parameter,  $\nu_s$ , is introduced to represent the fraction of sulphur content removed from the sulphur containing lumps. Their products,  $VGO\_low\_S_i$ ,  $LRES\_low\_S_i$  and  $HRES\_low\_S_i$ , contain the residual sulphur.

Product stoichiometric coefficients,  $\nu_{r,i}$ , for VGO and DIST from reaction 1 and 2 are estimated for the heaviest reacting lump. The lighter distributed lumps produce less VGO and DIST proportionally to their reacting lump molar mass. GAS and NAPH stoichiometric coefficients are calculated to complete the mass balance. Reactions 3 and 4 compete to

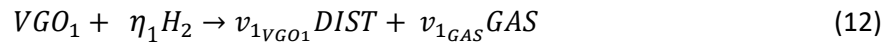
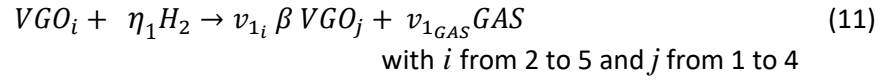
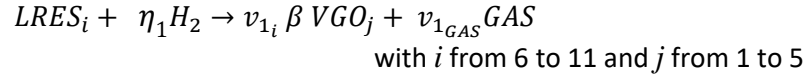
convert HRES<sub>i</sub> distributed lumps respectively into DIST and sediment with no secondary products. Reaction 5 is a cascade through LRES<sub>i</sub>, VGO<sub>i</sub> and DIST. Reaction 1 VGO product repartition coefficient,  $\beta_j$ , gives a linear distribution since there are up to 5 potential products.  $\beta_j$  is calculated by Eqn. (9) for lumps,  $i$ , VGO<sub>1</sub> to VGO<sub>N</sub> receiving reaction 1 product where  $N_{VGO}$  is the number of VGO product lumps and  $\alpha$  is the estimated parameter. So, if  $\alpha = 0$  the product is equally distributed between the VGO lumps.

$$\beta_j = \frac{1}{N_{VGO}} + \left( \frac{(N_{VGO} + 1)}{2} - j \right) \alpha \quad (9)$$



**Figure 7. Reaction scheme showing all reaction sets .**

Reaction 1: (10)



Reaction 2:



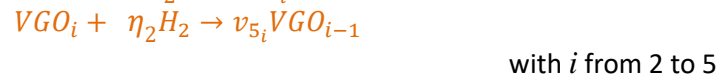
Reaction 3:



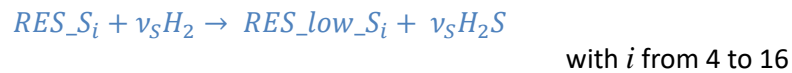
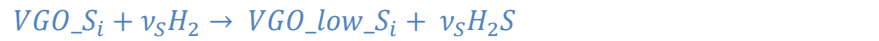
Reaction 4:



Reaction 5:



HDS reaction:



Temperature dependent cracking rates,  $r_{r,i}$ , in  $\text{mol.m}^{-3}.\text{s}^{-1}$ , are given by Eq.s (20) to (22) with thermal reactions 1 to 4 represented by Eq. (20) and catalytic reaction 5 by Eq. (21). The symbols,  $k_0$ , and,  $k_r$ , represent the reaction rate constant at the reference and reaction temperatures respectively.  $Ea_r$ , in  $\text{J.mol}^{-1}$ , is the activation energy,  $R$  the ideal gas constant and  $T$  the temperature in Kelvin.

$$r_{r,i} = \nu_{r,i} k_r C_i^{n_i} \quad \text{with } r = 1 \text{ to } 4 \quad (20)$$

$$r_{r,i} = \nu_{r,i} k_r C_i C_{H_2} \quad \text{with } r = 5 \quad (21)$$

$$\ln(k_r) = \ln(k_{0,r}) - \frac{Ea_r}{RT} \quad (22)$$

Catalytic cascade reaction 5 is first order with respect to the concentration of the distributed lump and  $H_2$ . Thermal reactions 3 and 4 are also first order with respect to the distributed lump concentrations. For thermal reactions 1 and 2, reaction orders,  $n$ , are calculated as shown in Eq. (23), where  $i$  corresponds to the distributed lump number for VGO<sub>1</sub> to LRES<sub>11</sub>. A reactivity parameter,  $f$ , is incorporated into the pre-exponential reaction constant as shown in Eq. (24). This gives a distribution of reaction rates increasing with boiling point as observed in the literature [58].

$$n = n_1 i + n_2 \quad (23)$$

$$k_{0,r,i} = k_{0,r} \exp(f \cdot i) \quad (24)$$

The HDS reaction rate is coupled to the hydroconversion rate as shown in Eq.s (25) and (26). Based on Figure 6, the relationship between hydroconversion and H<sub>2</sub>S is approximately linear and it is assumed that this can be extrapolated to all the distributed lumps and to the continuous reactor operating conditions.

$$\begin{array}{ll}
 i = 1 \text{ to } 5 & C_i = C_{VGO\_Si} + C_{VGO\_low\_Si} \\
 i = 6 \text{ to } 19 & C_i = C_{RES\_Si} + C_{RES\_low\_Si}
 \end{array} \quad (25)$$

$$\begin{array}{ll}
 \left. \begin{array}{l} r = 1, 5 \\ i = 1 \text{ to } 5 \end{array} \right\} & r_{HDS,r,i} = \frac{C_{VGO\_Si}}{C_i^L} r_{r,i} \\
 \left. \begin{array}{l} r = 1 \text{ to } 5 \\ i = 6 \text{ to } 19 \end{array} \right\} & r_{HDS,r,i} = \frac{C_{RES\_Si}}{C_i^L} r_{r,i}
 \end{array} \quad (26)$$

Finally, the H<sub>2</sub> consumption rate depends on reaction type with one general consumption rate parameter,  $\eta_1$ , for thermal reactions ( $r = 1$  to  $4$ ) and another,  $\eta_2$ , for the cascade reaction, ( $r = 5$ ).

### 3.3. Parameter estimation

Table 3 lists the 19 estimated parameters for the slurry phase hydroconversion kinetic model with recycle. The VGO product repartition parameter applies only to reaction set 1 and stoichiometric coefficients are only for reactions 1 and 2. Parameter estimation was carried out against the 1324 data points from the 74 experiments comprising the six later campaigns numbered, 7 to 12, because these include measurement of the produced sediment quantities and H<sub>2</sub> consumed. Campaigns 7 to 12 were all performed in recycle mode with both reactors in operation. The temperature range covered is 420 – 435°C. The data points are the total outlet mass flow rates of all the measured components, the NAPH and DIST boiling ranges and the distributed lumps. The sediment, H<sub>2</sub> and H<sub>2</sub>S data was weighted to compensate for low mass flow rates. MATLAB non-linear least squares solver function, lsqnonlin, was used with the trust-region-reflective algorithm which minimises an objective function based on an

input vector of differences between the measured and calculated data. Parameter significance levels and confidence limits were determined from Eq.s (27) to (29) [59].  $J$  is the Jacobian matrix and  $se(b_p)$  is the standard error found for each parameter.  $SSE$ ,  $n_d$  and  $p$  are the sum of the errors squared and the numbers of data points and parameters respectively.  $b_p$  is the parameter value,  $t_{obs}$  is the observed student t-value and  $\alpha_t/2$  is the significance level.

**Table 3. Parameters estimated for slurry phase hydroconversion kinetic model with recycle.**

	<u>Reactions</u>				
	<u>1</u>	<u>2</u>	<u>3</u>	<u>4</u>	<u>5</u>
<u>Reaction specific parameters:</u>					
Pre-exponential constants ( $\text{mol}^{-1}.\text{m}^3)^{n-1} .\text{s}^{-1}$ )	$\ln(k_1)$	$\ln(k_2)$	$\ln(k_3)$	$\ln(k_4)$	$\ln(k_5)^*$
Activation energies ( $\text{kJ}.\text{mol}^{-1}$ )	$Ea_1$	$Ea_2$	$Ea_3$	$Ea_4$	$Ea_5$
Stoichiometric coefficients (-)	$\nu_1$	$\nu_2$			
VGO product repartition (-)	$\alpha$				
H <sub>2</sub> consumption rate parameter (catalytic reaction) (-)					$\eta_2$
<u>General parameters:</u>					
Reaction order (-)	$n_1 \quad n_2$				
Reactivity parameter (-)	$f$				
H <sub>2</sub> consumption rate parameter (thermal reaction) (-)	$\eta_1$				
Sulphur fraction removed (-)	$\nu_{HDS}$				
	* $(\text{mol}^{-1}.\text{m}^3)^n .\text{s}^{-1}$				

$$se(b_p) = \sqrt{\frac{SSE (J^T J)^{-1}_{pp}}{(n_d - p)}} \quad (27)$$

$$t_{obs} = \frac{b_p}{se(b_p)} \quad (28)$$

$$b_p \pm se(b_p)t(n_d - p; \alpha_t/2) \quad (29)$$

#### 4. Results and Discussion

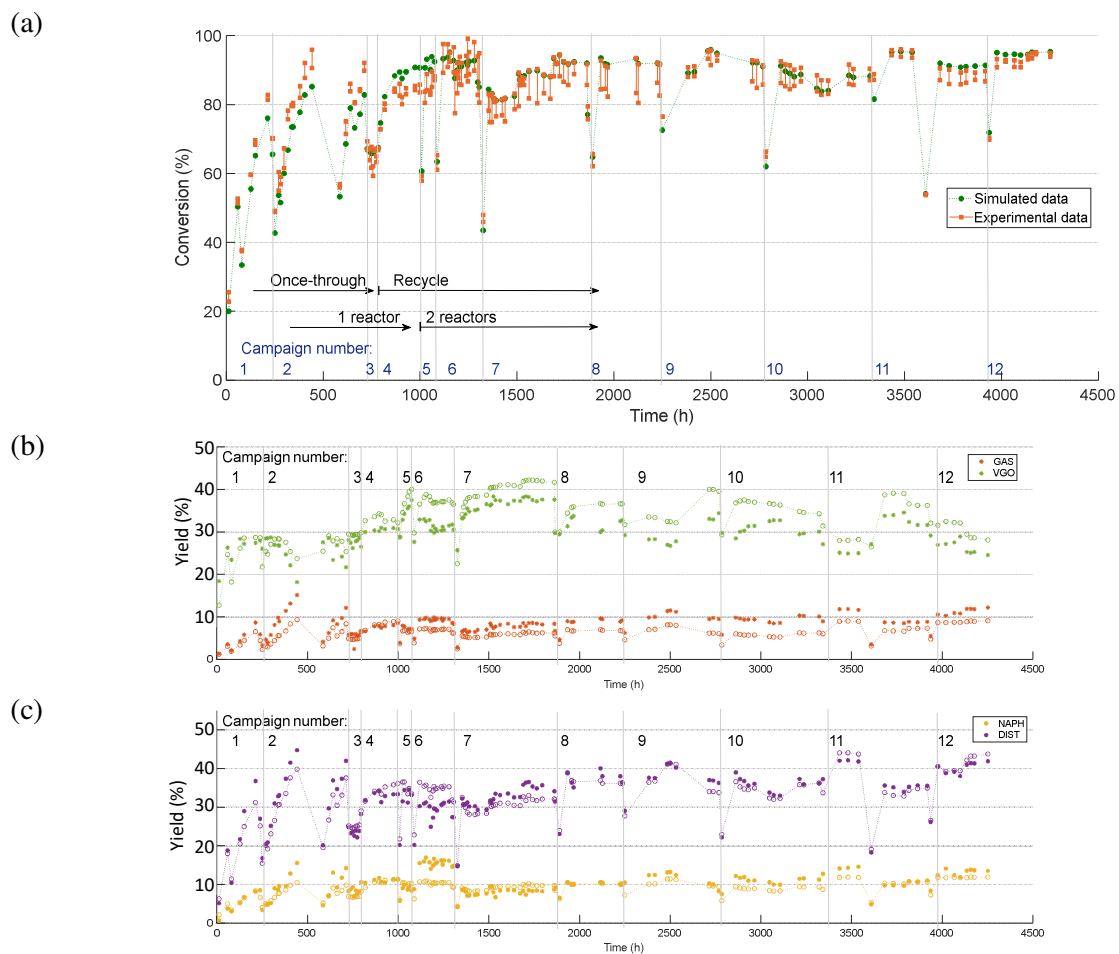
Table 4 gives the estimated parameters and corresponding 95% confidence limits. The reaction constants are in the form of their natural logs at the reference temperature  $\ln(k_{0,r})$ . All the parameters are significant to 95% except for  $\eta_2$ , the stoichiometric coefficient for H<sub>2</sub> consumption applied to reaction set 5, the catalytic cascade. The activation energy confidence limits are quite wide for reactions 4 and 5, perhaps because the temperature range of the data selected for parameter estimation is quite narrow and also, catalytic reaction 5 is not very temperature sensitive. It is interesting to compare the new parameter values with those from our previous work at lower conversions with a Safaniya VR in a semi-batch reactor [36]. The value of the VGO product repartition parameter,  $\alpha$ , is unchanged and indicates that reaction 1 produces 2.13 times more VGO<sub>1</sub> than VGO<sub>5</sub>. The estimated reaction 1 and 2 order parameters,  $n_1$  and  $n_2$ , correspond to reaction orders decreasing from 3.60 to 2.45 as the distributed lumps, VGO<sub>1</sub> through RES<sub>6</sub> get heavier. This agrees with our previous work [36] and is coherent with the increased value of the reactivity parameter,  $f$ , to 1.22 from 0.845 and the idea that lighter distributed lumps become more heterogeneous by receiving more hydroconversion products with a wide range of structures. The estimated activation energies at deep hydroconversion for reactions 1 to 3 are all high relative to our previous results at

moderate conversions, respectively 289, 334 and 306 kJ.mol<sup>-1</sup> for the same reactions in a semi-batch reactor [36]. Finally, the stoichiometric coefficient for reaction 1 is unchanged, but that of reaction 2 has adjusted to account for the inclusion of reaction 4, HRES to sediment.

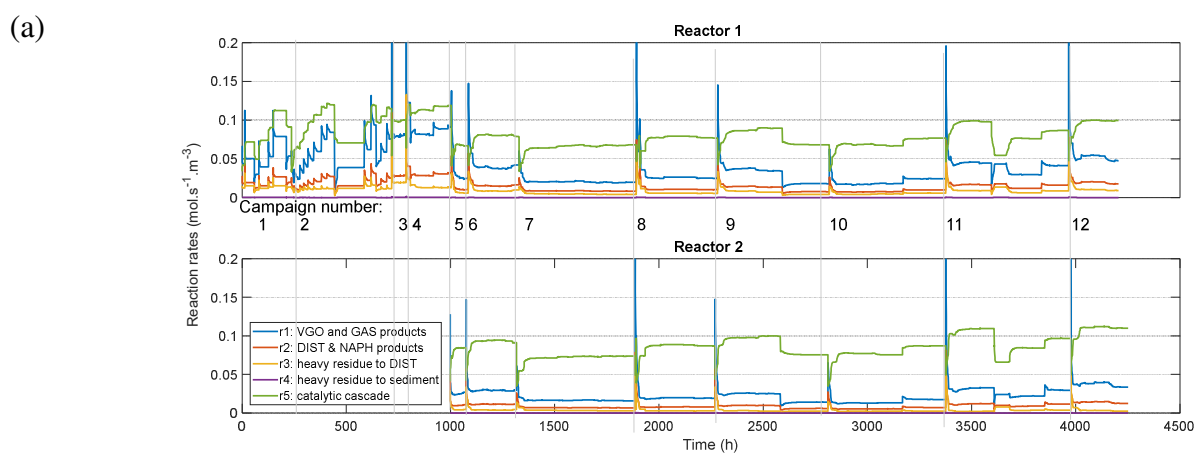
Figure 8 (a) shows the experimental conversions for all the experiments compared against those calculated with the estimated parameters. There is a good fit for the experiments used to estimate the parameters, campaigns 7 to 12. Campaigns 1 to 3 were performed with a single reactor in once-through mode. The recycle was introduced from campaign 4 and the second reactor from campaign 5. The first experiment of each campaign was performed in once-through mode at these experiments stand out because of their low conversion rates. The results validate the estimated parameters but the conversion is consistently underestimated for the pilot in once-through mode. It is well known that the small amount of residue remaining at the very high conversions obtained in recycle mode is less reactive than that found in VR feedstock. The rate equations for reaction sets 1 and 2 are designed to take this into account by inclusion of a reaction order distribution but reactions 3, 4 and 5 are all first order. Figure 8 (b) and (c) compare the calculated and experimental yields for VGO, GAS and NAPH and DIST. Figure 9 (a) gives the calculated reaction rates for all the campaigns. It shows that at very high conversions it is the catalytic cascade reaction which dominates. Unlike reaction sets 1 and 2, the catalytic cascade is a first order reaction and therefore does not take any heterogeneity within the distributed lumps into account. So this could be the cause of the discrepancy observed between the measured and calculated conversions in once-through mode. This result corresponds well with the knowledge that it is the catalytic slurry phase hydroconversion processes that achieve very high conversions; once all the material that can be consumed by the thermal reactions is gone, catalytic reactions continue to erode the remaining refractory molecules. Figure 9 (b) and (c) show the calculated concentrations.

Table 4. Estimated parameter values for slurry phase hydroconversion kinetic model with recycle

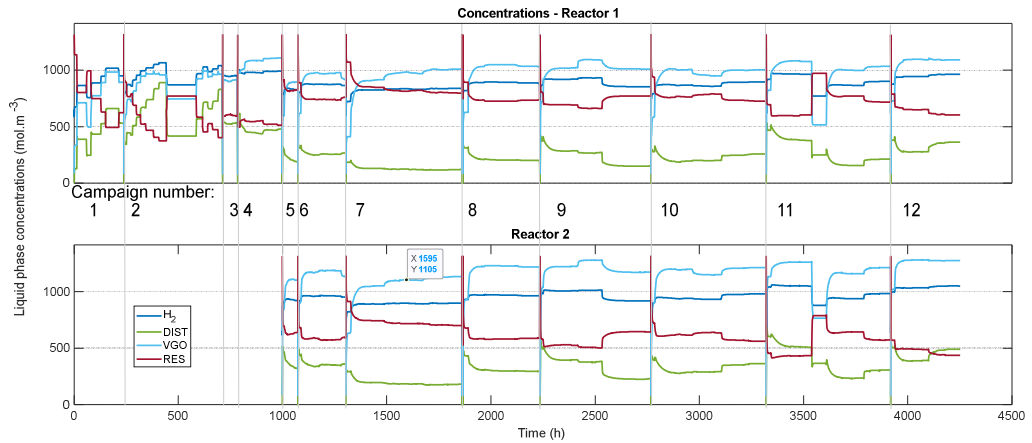
<u>Reaction specific parameters</u>					
<u>Reaction</u>	$\ln(k_0)$	$Ea$	$\nu$	$\alpha$	$\eta_2$
	$(\text{mol}^{-1}.\text{m}^3)^{n-1} .\text{s}^{-1}$	$(\text{kJ}.\text{mol}^{-1})$	(-)	(-)	(-)
1	$-28.4 \pm 0.5$	$410 \pm 13$	$5.07 \pm 0.09$	$0.036 \pm 0.012$	
2	$-29.3 \pm 0.5$	$376 \pm 13$	$4.37 \pm 0.46$		
3	$-8.43 \pm 0.09$	$366 \pm 5$			
4	$-12.6 \pm 0.5$	$299 \pm 29$			
5	$-16.70 \pm 0.04^*$	$79 \pm 10$			$0.4 \pm 0.7$
					$*(\text{mol}^{-1}.\text{m}^3)^n .\text{s}^{-1}$
<u>General parameters</u>					
$n_1$	$-0.115 \pm 0.040$				
$n_2$	$3.717 \pm 0.198$				
$f$	$1.220 \pm 0.143$				
$\eta_1$	$5.992 \pm 1.287$				
$\nu_{HDS}$	$0.859 \pm 0.039$				



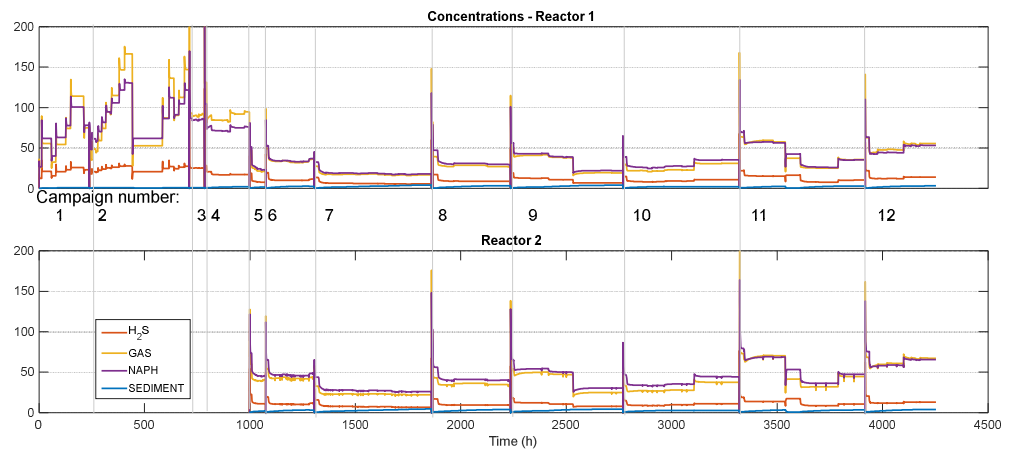
**Figure 8. Calculated and experimental (a) conversions (b) VGO and GAS yields (c) NAPH and DIST yields for all the campaigns.**



(b)

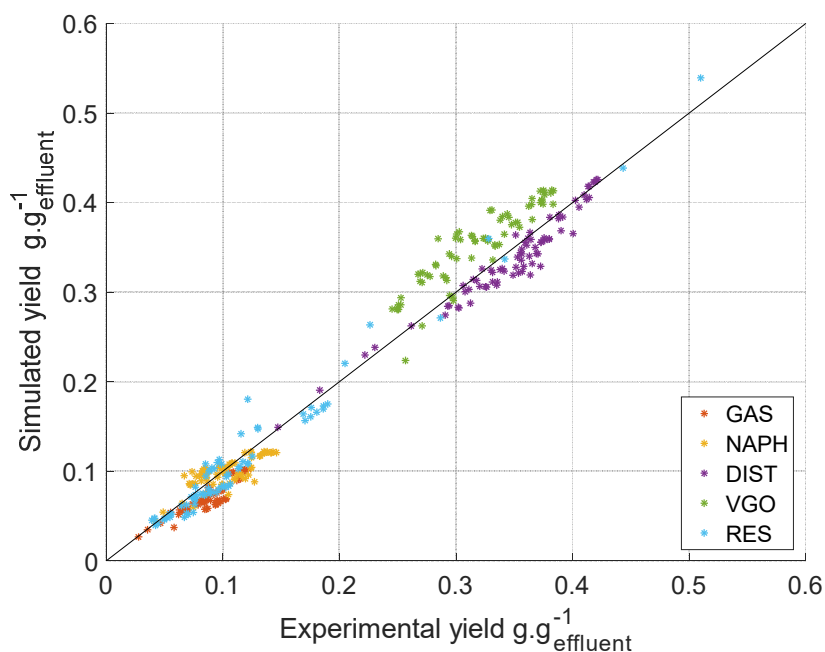


(c)



**Figure 9. Calculated (a) reaction rates and (b), (c) concentrations for all campaigns .**

Figure 10 shows the yields parity plot for GAS, NAPH and DIST and the overall VGO and residue lumps. The yields fit well except for the VGO which is slightly overestimated. At deep conversion, the VGO product is more reactive than the model predicts. This is probably due to ageing and, as for the discrepancy in the once-through mode conversions, could be a consequence of representing reaction 5 as first order.



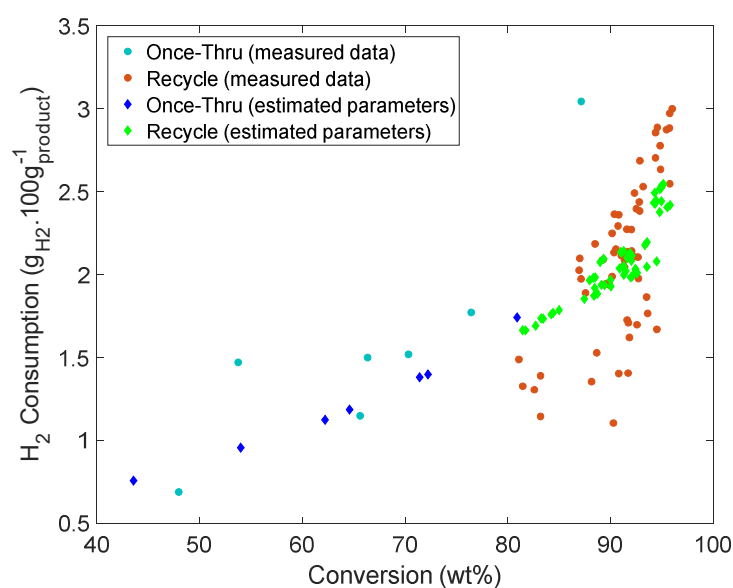
**Figure 10. Yields parity plot for GAS, NAPH and DIST and the overall VGO and residue lumps.**

Figure 11 shows the experimental and calculated  $H_2$  consumption against conversion. The very simple  $H_2$  consumption model with only two parameters, one representing  $H_2$  uptake by the thermal reactions and the other by the catalytic cascade has resulted in a much narrower variance than for the measured data. The parameters give a good idea of the average  $H_2$  stoichiometric coefficient across all the reactions but more detail is needed to observe the mechanisms at play. Also, the  $H_2$  consumption rate is much lower than in our previous work with a Safaniya VR [36].  $H_2$  consumption depends on the molecular structures undergoing hydroconversion, whereas our distributed lumps are defined by true boiling point only. If we compare the two VRs, the Iran Heavy has lower total hydrogen content than the Safaniya, more aromatics and less resins, with reported atomic H/C ratios of 1.44 [60] and 1.5 [61] respectively. So, the Safaniya does not seem to lack hydrogen. However, Saturates, Aromatics, Resins and Asphaltenes (SARA) analysis results from the literature, given in Table 5, indicate that Safaniya VR is richer in Resins and Asphaltenes and, therefore, it may be the cracking reactions associated with these species which consume more hydrogen. The

main conclusion that can be drawn is that H<sub>2</sub> consumption is highly dependent on feedstock composition. To consider the impact of this on the model, the cascade reaction rate depends on H<sub>2</sub> concentration whilst thermal reaction rates are independent of it. However, reactor H<sub>2</sub> concentrations are more likely to be controlled by the reactor operating pressure than the reaction rates. So, the likely outcome of modeling with the reported parameters would be a misrepresentation of H<sub>2</sub> requirements, and the best option would be to adjust the H<sub>2</sub> consumption parameters for the new feedstock. If the H<sub>2</sub> partial pressure in the reactor was reduced, the catalytic cascade reaction rate would decrease and the reaction profile would shift towards more thermal reactions.

**Table 5. SARA fractions of Iran Heavy and Safaniya VRs**

	Saturates	Aromatics	Resins	Asphaltenes
Iran Heavy [60]	12.6	46.7	29.9	10.8
Safaniya [62]	11	39	34	14



**Figure 11. Experimental and calculated H<sub>2</sub> consumption against conversion.**

Figure 12 (a) gives the parity plot between the calculated and experimental values for sediment yield and Figure 12 (b) shows the calculated sediment concentration in the reactors. The model results are of correct order although there is some scatter. According to our model, sediment production from heavy residue does not have time to stabilise under recycle operation and sediment accumulates in the reactors. **Figure 13** shows the H<sub>2</sub>S yield parity plot with good results in both once-through and recycle modes. This validates the linear approach to modelling the relation between hydroconversion and HDS.

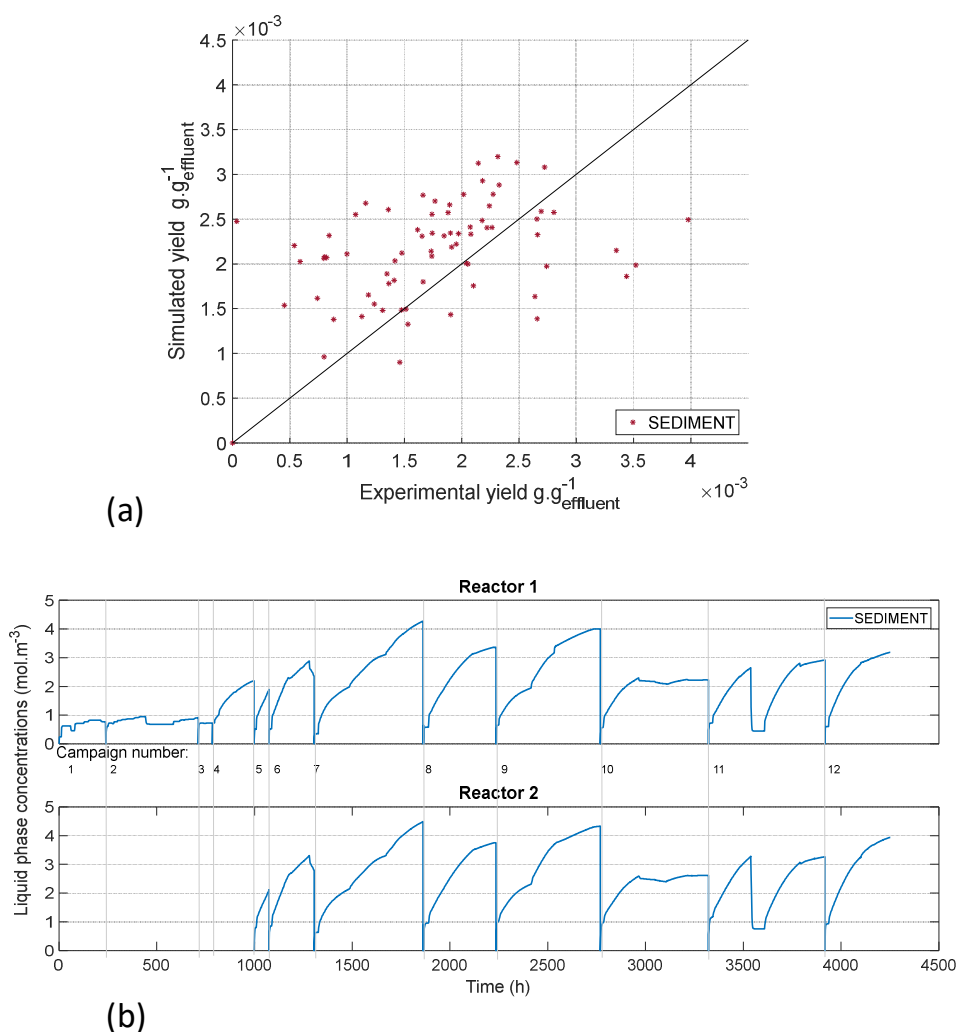


**Figure 12. Sediment (a) yield parity plot (b) reactor calculated concentration**

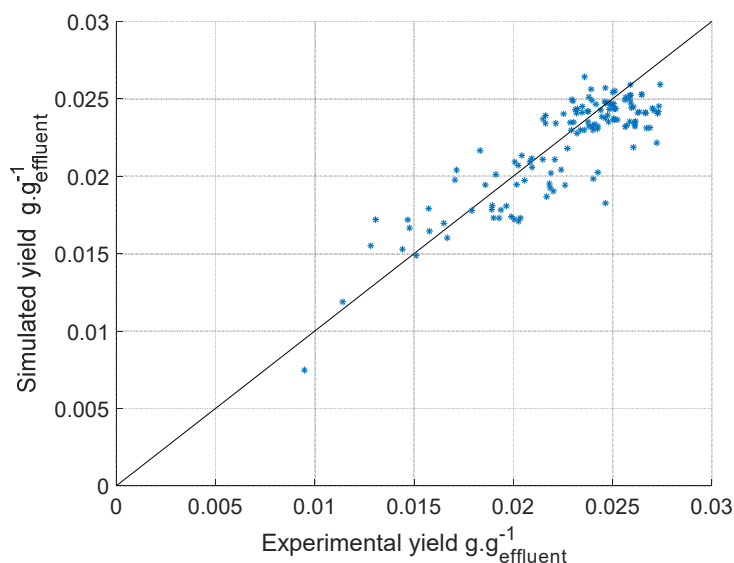


**Figure 13. H<sub>2</sub>S yield parity plot.**

## 5. Conclusions

The distributed lump model of VGO and RES for slurry phase VR hydroconversion has been extended to include sediment production and give a more physical representation of HDS. The new version of the model has been tested against deep hydroconversion data from a continuous pilot plant with recycle. The linear approach to integrating the HDS reaction has been validated against the experimental data and the sediment production results indicate an accumulation in the reactor in recycle operating mode. The reaction regime under the deep hydroconversion conditions found in recycle operating mode shifts away from thermal reactions and towards the catalytic cascade. This reaction should be the focus in adapting this kinetic model to represent the full operating range of an industrial slurry phase hydroconversion unit.

## Acknowledgements

The authors would like thank TOTAL for financial support.

## Nomenclature

$a, b$	Parameters for gas volume correlation (-)
$A, B$	Parameters for Riazi extrapolation method [57] (-)
$C$	Concentration ( $\text{mol.m}^{-3}$ )
$E_a$	Activation energy ( $\text{kJ.mol}^{-1}$ )
$f$	Reactivity parameter (-)
$F_{ex}$	Vapour liquid mass transfer rates ( $\text{mol.s}^{-1}$ )
$k$	Reaction rate constant
$k_{la}$	Vapour –liquid mass transfer coefficient( $\text{s}^{-1}$ )
$n$	Reaction order (-), reaction order parameter (-)
$N_{VGO}$	Number of VGO product lumps
$Q_v$	Volumetric flow rate ( $\text{m}^3.\text{s}^{-1}$ )
$r$	Reaction rate ( $\text{mol.s}^{-1}.\text{m}^{-3}$ )
$R$	Ideal gas constant ( $\text{kJ.mol}^{-1}.\text{K}^{-1}$ )
$t$	Time (s)
$T$	Temperature (K)
$T_b$	Boiling point ( $^{\circ}\text{C}$ , K)
$T_{b0}$	Initial boiling point (K)
$V$	Volume ( $\text{m}^3$ )
$V_{mol}$	Molar volume ( $\text{mol.m}^{-3}$ )
$x_c$	Distilled fraction (-)
$\alpha$	Parameter for repartition coefficient for reaction 1VGO product (-)
$\varepsilon_g$	Volumetric gas fraction
$\beta$	Repartition coefficient for reaction 1VGO product (-)
$\eta_1, \eta_2$	$\text{H}_2$ consumption rate parameters (-), (-)

$v$  Stoichiometric coefficient (-)

Subscripts/superscripts

$g$  Gas phase

$i,j$  Lump

$L$  Liquid phase

$r$  Reaction

$T$  total

$0$  Reference temperature

## References

- [1] International Energy Agency, World Energy Outlook 2018, OECD, 2018.  
<https://doi.org/10.1787/weo-2018-en>.
- [2] A. Marafi, H. Albazzaz, M.S. Rana, Hydroprocessing of heavy residual oil: Opportunities and challenges, *Catal. Today*. 329 (2019) 125–134.  
<https://doi.org/10.1016/j.cattod.2018.10.067>.
- [3] M.J. Angeles, C. Leyva, J. Ancheyta, S. Ramírez, A review of experimental procedures for heavy oil hydrocracking with dispersed catalyst, *Catal. Today*. 220–222 (2014) 274–294. <https://doi.org/10.1016/j.cattod.2013.08.016>.
- [4] R. Sahu, B.J. Song, J.S. Im, Y.-P. Jeon, C.W. Lee, A review of recent advances in catalytic hydrocracking of heavy residues, *J. Ind. Eng. Chem.* 27 (2015) 12–24.  
<https://doi.org/10.1016/j.jiec.2015.01.011>.
- [5] S. Zhang, D. Liu, W. Deng, G. Que, A Review of Slurry-Phase Hydrocracking Heavy Oil Technology, *Energy Fuels*. 21 (2007) 3057–3062. <https://doi.org/10.1021/ef700253f>.
- [6] I. Alawad, I. Al Zubaidi, Advances in Upgrading Process of Petroleum Residue: A Review, *Eur. J. Eng. Res. Sci.* 4 (2019) 104–110.  
<https://doi.org/10.24018/ejers.2019.4.6.1123>.
- [7] J. Sánchez, A. Moreno, F. Mondragón, K.J. Smith, Bifunctional MoS<sub>2</sub>-Silica-Alumina Catalysts for Slurry Phase Phenanthrene-Decalin Hydroconversion, *Energy Fuels*. 32 (2018) 10910–10922. <https://doi.org/10.1021/acs.energyfuels.8b02770>.
- [8] K.-D. Kim, Y.-K. Lee, Active phase of dispersed MoS<sub>2</sub> catalysts for slurry phase hydrocracking of vacuum residue, *J. Catal.* 369 (2019) 111–121.  
<https://doi.org/10.1016/j.jcat.2018.10.013>.
- [9] M.Kh. Kadieva, A.L. Maximov, K.M. Kadiev, Ex-Situ Synthesis and Study of Nanosized Mo-Containing Catalyst for Petroleum Residue Hydro-Conversion, *Catalysts*. 9 (2019) 649. <https://doi.org/10.3390/catal9080649>.
- [10] L.C. Castañeda, J.A.D. Muñoz, J. Ancheyta, Current situation of emerging technologies for upgrading of heavy oils, *Catal. Today*. 220–222 (2014) 248–273.  
<https://doi.org/10.1016/j.cattod.2013.05.016>.

- [11] T.A. Al-Attas, S.A. Ali, M.H. Zahir, Q. Xiong, S.A. Al-Bogami, Z.O. Malaibari, S.A. Razzak, M.M. Hossain, Recent Advances in Heavy Oil Upgrading Using Dispersed Catalysts, *Energy Fuels*. 33 (2019) 7917–7949. <https://doi.org/10.1021/acs.energyfuels.9b01532>.
- [12] G. Bellussi, G. Rispoli, A. Landoni, R. Millini, D. Molinari, E. Montanari, D. Moscotti, P. Pollesel, Hydroconversion of heavy residues in slurry reactors: Developments and perspectives, *J. Catal.* 308 (2013) 189–200. <https://doi.org/10.1016/j.jcat.2013.07.002>.
- [13] K.H. Kang, G.T. Kim, S. Park, P.W. Seo, H. Seo, C.W. Lee, A review on the Mo-precursors for catalytic hydroconversion of heavy oil, *J. Ind. Eng. Chem.* 76 (2019) 1–16. <https://doi.org/10.1016/j.jiec.2019.03.022>.
- [14] K. Niemann, F. Wenzel, The VEBA-COMBI-CRACKING-Technology: An update, *Fuel Process. Technol.* 35 (1993) 1–20. [https://doi.org/10.1016/0378-3820\(93\)90082-F](https://doi.org/10.1016/0378-3820(93)90082-F).
- [15] M.M. Ramírez-Corredores, The science and technology of unconventional oils: finding refining opportunities, Elsevier ; Academic Press, an imprint of Elsevier, London, United Kingdom, 2017.
- [16] C.J. Calderón, J. Ancheyta, Modeling of CSTR and SPR small-scale isothermal reactors for heavy oil hydrocracking and hydrotreating, *Fuel*. 216 (2018) 852–860. <https://doi.org/10.1016/j.fuel.2017.11.089>.
- [17] A. Matsumura, S. Sato, T. Kondo, I. Saito, W. Desouza, Hydrocracking Marlim vacuum residue with natural limonite. Part 2: experimental cracking in a slurry-type continuous reactor, *Fuel*. 84 (2005) 417–421. <https://doi.org/10.1016/j.fuel.2004.09.015>.
- [18] G. Noguera, S. Araujo, J. Hernández, A. Rivas, D. Mendoza, O. Castellano, A comparative activity study of a new ultra-dispersed catalyst system for a hydrocracking/hydrotreating technology using vacuum residue oil: Merrey/Mesa, *Chem. Eng. Res. Des.* 90 (2012) 1979–1988. <https://doi.org/10.1016/j.cherd.2012.04.006>.
- [19] Kh.M. Kadiev, L.A. Zekel', M.Kh. Kadieva, S.N. Khadzhev, Formation of Polycondensation Products in Heavy Oil Feedstock Hydroconversion in the Presence of Ultrafine Catalyst: Physicochemical Study, *Pet. Chem.* 58 (2018) 519–527. <https://doi.org/10.1134/S0965544118070034>.
- [20] D.-W. Kim, C.-H. Lee, Efficient conversion of extra-heavy oil into distillates using tetralin/activated carbon in a continuous reactor at elevated temperatures, *J. Anal. Appl. Pyrolysis*. 140 (2019) 245–254. <https://doi.org/10.1016/j.jaap.2019.04.001>.
- [21] I. Morawski, J. Mosio-Mosiewski, Effects of parameters in Ni–Mo catalysed hydrocracking of vacuum residue on composition and quality of obtained products, *Fuel Process. Technol.* 87 (2006) 659–669. <https://doi.org/10.1016/j.fuproc.2006.01.006>.
- [22] M.M. Fathi, P. Pereira-Almao, Catalytic Aquaprocessing of Arab Light Vacuum Residue via Short Space Times, *Energy Fuels*. 25 (2011) 4867–4877. <https://doi.org/10.1021/ef200936k>.
- [23] F.A. Cabrales-Navarro, P. Pereira-Almao, Catalytic Steam Cracking of a Deasphalted Vacuum Residue Using a Ni/K Ultradispersed Catalyst, *Energy Fuels*. 31 (2017) 3121–3131. <https://doi.org/10.1021/acs.energyfuels.6b03004>.
- [24] R.G. Kukushkin, P.M. Elets'kii, O.O. Zaikina, G.A. Sosnin, O.A. Bulavchenko, V.A. Yakovlev, Studying the Steam Cracking of Heavy Oil over Iron- and Molybdenum-Containing Dispersed Catalysts in a Flow-Type Reactor, *Catal. Ind.* 10 (2018) 344–352. <https://doi.org/10.1134/S2070050418040104>.
- [25] T. Jansen, D. Guerry, D. Gotteland, R. Bacaud, M. Lacroix, M. Ropars, C. Lorentz, C. Geantet, M. Tayakout-Fayolle, Characterization of a continuous micro-scale pilot unit for petroleum residue hydroconversion with dispersed catalysts: Hydrodynamics and

- performances in once-through and recycling mode, *Chem. Eng. J.* 253 (2014) 493–501. <https://doi.org/10.1016/j.cej.2014.05.032>.
- [26] T. Jansen, D. Guerry, E. Leclerc, M. Ropars, M. Lacroix, C. Geantet, M. Tayakout-Fayolle, Simulation of Petroleum Residue Hydroconversion in a Continuous Pilot Unit Using Batch Reactor Experiments and a Cold Mock-Up, *Ind. Eng. Chem. Res.* 53 (2014) 15852–15861. <https://doi.org/10.1021/ie502242f>.
- [27] P. Alvarez, B. Browning, M. Lacroix, T. Jansen, E. Leclerc, C. Geantet, M. Tayakout-Fayolle, Impact of Unconverted Residue Recycling on Slurry-Phase Hydroconversion Performance in a Continuous Microscale Pilot Unit, *Energy Fuels*. 34 (2020) 4183–4193. <https://doi.org/10.1021/acs.energyfuels.9b04519>.
- [28] S. Japanwala, K.H. Chung, H.D. Dettman, M.R. Gray, Quality of Distillates from Repeated Recycle of Residue, *Energy Fuels*. 16 (2002) 477–484. <https://doi.org/10.1021/ef010234j>.
- [29] A. Del Bianco, N. Panariti, M. Marchionna, Upgrading Activity of Recycled Mo-Based Dispersed Catalysts, *Am. Chem. Soc. Div Petr Chem.* 42 (1997) 484–488.
- [30] J. Zhou, W. Deng, D. Liu, S. Liang, G. Que, Effect of vacuum bottom recycling on slurry bed hydrocracking of residue, *Acta Pet. Sin. Process. Sect.* 17 (2001) 82–85.
- [31] R.G. Tailleux, Effect of recycling the unconverted residue on a hydrocracking catalyst operating in an ebullated bed reactor, *Fuel Process. Technol.* 88 (2007) 779–785. <https://doi.org/10.1016/j.fuproc.2007.03.011>.
- [32] K.M. Kadiev, O.V. Zaytseva, E.E. Magomadov, E.A. Chernysheva, N.V. Oknina, A.E. Batov, M.K. Kadieva, V.M. Kapustin, S.N. Khadzhiev, Structural transformations of asphaltenes during hydroconversion of vacuum residue with recycling the hydroconversion product distillation residue, *Pet. Chem.* 55 (2015) 487–496. <https://doi.org/10.1134/S0965544115060067>.
- [33] Shi, B and Que, G, Chemical structure change of recycling vacuum bottom residue from slurry-bed hydrocracking of Karamay atmospheric residue in the pilot plant p718-721, 2003.
- [34] G. Bellussi, G. Rispoli, D. Molinari, A. Landoni, P. Pollesel, N. Panariti, R. Millini, E. Montanari, The role of MoS<sub>2</sub> nano-slabs in the protection of solid cracking catalysts for the total conversion of heavy oils to good quality distillates, *Catal Sci Technol.* 3 (2013) 176–182. <https://doi.org/10.1039/C2CY20448G>.
- [35] A. Quitian, J. Ancheyta, Experimental Methods for Developing Kinetic Models for Hydrocracking Reactions with Slurry-Phase Catalyst Using Batch Reactors, *Energy Fuels*. 30 (2016) 4419–4437. <https://doi.org/10.1021/acs.energyfuels.5b01953>.
- [36] B. Browning, I. Pitault, F. Couenne, T. Jansen, M. Lacroix, P. Alvarez, M. Tayakout-Fayolle, Distributed lump kinetic modeling for slurry phase vacuum residue hydroconversion, *Chem. Eng. J.* 377 (2019) 119811. <https://doi.org/10.1016/j.cej.2018.08.197>.
- [37] T.S. Nguyen, M. Tayakout-Fayolle, M. Ropars, C. Geantet, Hydroconversion of an atmospheric residue with a dispersed catalyst in a batch reactor: Kinetic modeling including vapor–liquid equilibrium, *Chem. Eng. Sci.* 94 (2013) 214–223. <https://doi.org/10.1016/j.ces.2013.02.036>.
- [38] J. Ancheyta, S. Sánchez, M.A. Rodríguez, Kinetic modeling of hydrocracking of heavy oil fractions: A review, *Catal. Today*. 109 (2005) 76–92. <https://doi.org/10.1016/j.cattod.2005.08.015>.
- [39] J.W. Thybaut, G.B. Marin, Multiscale Aspects in Hydrocracking, in: *Adv. Catal.*, Elsevier, 2016: pp. 109–238. <https://doi.org/10.1016/bs.acat.2016.10.001>.

- [40] S.R. Horton, Z. Hou, B.M. Moreno, C.A. Bennett, M.T. Klein, Molecule-based modeling of heavy oil, *Sci. China Chem.* 56 (2013) 840–847. <https://doi.org/10.1007/s11426-013-4895-8>.
- [41] L. Zhang, Z. Hou, S.R. Horton, M.T. Klein, Q. Shi, S. Zhao, C. Xu, Molecular Representation of Petroleum Vacuum Resid, *Energy Fuels.* 28 (2014) 1736–1749. <https://doi.org/10.1021/ef402081x>.
- [42] S.R. Horton, L. Zhang, Z. Hou, C.A. Bennett, M.T. Klein, S. Zhao, Molecular-Level Kinetic Modeling of Resid Pyrolysis, *Ind. Eng. Chem. Res.* 54 (2015) 4226–4235. <https://doi.org/10.1021/ie5041572>.
- [43] R.I. Rueda-Velásquez, M.R. Gray, Monte Carlo Simulation of Asphaltenes and Products from Thermal Cracking, *Energy Fuels.* 28 (2014) 2352–2364. <https://doi.org/10.1021/ef402390w>.
- [44] L.P. de Oliveira, J.J. Verstraete, M. Kolb, Simulating vacuum residue hydroconversion by means of Monte-Carlo techniques, *Catal. Today.* 220–222 (2014) 208–220. <https://doi.org/10.1016/j.cattod.2013.08.011>.
- [45] T.T.H. Nguyen, S. Teratani, R. Tanaka, A. Endo, M. Hirao, Development of a Structure-Based Lumping Kinetic Model for Light Gas Oil Hydrodesulfurization, *Energy Fuels.* 31 (2017) 5673–5681. <https://doi.org/10.1021/acs.energyfuels.7b00360>.
- [46] Z. Chen, S. Feng, L. Zhang, Q. Shi, Z. Xu, S. Zhao, C. Xu, Molecular-level kinetic modelling of fluid catalytic cracking slurry oil hydrotreating, *Chem. Eng. Sci.* 195 (2019) 619–630. <https://doi.org/10.1016/j.ces.2018.10.007>.
- [47] C.J. Calderón, J. Ancheyta, Modeling, simulation, and parametric sensitivity analysis of a commercial slurry-phase reactor for heavy oil hydrocracking, *Fuel.* 244 (2019) 258–268. <https://doi.org/10.1016/j.fuel.2019.01.138>.
- [48] R.I. Rueda-Velásquez, M.R. Gray, A viscosity-conversion model for thermal cracking of heavy oils, *Fuel.* 197 (2017) 82–90. <https://doi.org/10.1016/j.fuel.2017.02.020>.
- [49] B.E. Stangeland, A Kinetic Model for the Prediction of Hydrocracker Yields, *Ind. Eng. Chem. Process Des. Dev.* 13 (1974) 71–76. <https://doi.org/10.1021/i260049a013>.
- [50] C.S. Laxminarasimhan, R.P. Verma, P.A. Ramachandran, Continuous lumping model for simulation of hydrocracking, *AIChE J.* 42 (1996) 2645–2653. <https://doi.org/10.1002/aic.690420925>.
- [51] M.A. Pacheco, C.G. Dassori, Hydrocracking: An improved Kinetic Model and Reactor Modeling, *Chem. Eng. Commun.* 189 (2002) 1684–1704. <https://doi.org/10.1080/00986440214584>.
- [52] S. Mohanty, D.N. Saraf, D. Kunzru, Modeling of a hydrocracking reactor, *Fuel Process. Technol.* 29 (1991) 1–17. [https://doi.org/10.1016/0378-3820\(91\)90013-3](https://doi.org/10.1016/0378-3820(91)90013-3).
- [53] G. Li, Y. Xia, W. Zeng, Kinetic mechanism research of an industrial hydrocracker based on strict calculation of stoichiometric coefficients, *Fuel.* 103 (2013) 285–291. <https://doi.org/10.1016/j.fuel.2012.09.044>.
- [54] H. Harode, M. Ramteke, Axial dispersion modeling of industrial hydrocracking unit and its multiobjective optimization, *Chem. Eng. Res. Des.* 121 (2017) 57–68. <https://doi.org/10.1016/j.cherd.2017.02.033>.
- [55] ASTM D7169-16, Standard Test Method for Boiling Point Distribution of Samples with Residues Such as Crude Oils and Atmospheric and Vacuum Residues by High Temperature Gas Chromatography, (2016). [www.astm.org](http://www.astm.org).
- [56] A. Vickers, Higher-Temperature Simulated Distillation with DB-HT Sim Dis Columns: Application, *Hydrocarbon Processing*, (2002). <https://www.agilent.com/cs/library/applications/5988-7929EN.pdf> (accessed March 12, 2018).

- [57] M.R. Riazi, Characterization and properties of petroleum fractions, ASTM International, W. Conshohocken, PA, 2005.
- [58] J. Weitkamp, The Influence of Chain Length in Hydrocracking and Hydroisomerization of *n*-Alkanes, in: J.W. Ward, S.A. Qader (Eds.), Hydrocracking Hydrotreating, AMERICAN CHEMICAL SOCIETY, WASHINGTON, D. C., 1975: pp. 1–27. <https://doi.org/10.1021/bk-1975-0020.ch001>.
- [59] A. Rasmuson, B. Andersson, L. Olsson, R. Andersson, Mathematical Modeling in Chemical Engineering, Cambridge University Press, 2014.
- [60] S. Zhao, Z. Xu, C. Xu, K.H. Chung, Feedstock characteristic index and critical properties of heavy crudes and petroleum residua, J. Pet. Sci. Eng. 41 (2004) 233–242. [https://doi.org/10.1016/S0920-4105\(03\)00157-8](https://doi.org/10.1016/S0920-4105(03)00157-8).
- [61] M. Thomas, B. Fixari, P. Leperchec, Y. Princic, L. Lena, Visbreaking of Safaniya vacuum residue in the presence of additives, Fuel. 68 (1989) 318–322. [https://doi.org/10.1016/0016-2361\(89\)90095-1](https://doi.org/10.1016/0016-2361(89)90095-1).
- [62] G. Magendie, B. Guichard, D. Espinat, Effect of acidity, hydrogenating phases and texture properties of catalysts on the evolution of asphaltenes structures during residue hydroconversion, Catal. Today. 258 (2015) 304–318. <https://doi.org/10.1016/j.cattod.2014.10.023>.